# Residue G346 in Transmembrane Segment Six is Involved in Inter-Domain Communication in P-Glycoprotein†

Janet Storm,‡ Megan L. O'Mara,|| Emily H. Crowley,‡ Jonathan Peall,‡ D. Peter Tieleman,|| Ian D. Kerr,§ and Richard Callaghan*,‡

*Nuffield Department of Clinical Laboratory Sciences, John Radcliffe Hospital, University of Oxford, Oxford OX3 9DU, United Kingdom, Centre for Biochemistry and Cell Biology, School of Biomedical Sciences, University of Nottingham, Queen's Medical Centre, Nottingham NG7 2UH, United Kingdom, and Department of Biological Sciences, University of Calgary, 2500 University Drive NW, Calgary, Alberta T2N 1N4, Canada*

*Received March 6, 2007; Revised Manuscript Received July 5, 2007*

ABSTRACT: Multidrug transporters such as P-glycoprotein require considerable inter-domain communication to couple energy utilization with substrate translocation. Elucidation of the regions or residues involved in these communication pathways is a key step in the eventual molecular description of multidrug transport. We used cysteine-scanning mutagenesis to probe the functional involvement of residues along the cytoplasmic half of transmembrane segment 6 (TM6) and its extension toward the nucleotide binding domain. The mutation of one residue (G346C) in this segment adversely affected drug transport in cells. Further investigation using purified protein revealed that the underlying biochemical effect was a reduction in basal ATP hydrolysis. This G346C mutation also affected the stimulation of ATPase activity in a drug dependent manner but had no effect on drug binding, ATP binding, or ADP release. Homology modeling of P-glycoprotein indicated that the G346C mutation caused a steric interaction between TM5 and TM6, thereby precluding a helical movement required to support ATP hydrolysis.

Multidrug efflux pumps are characterized by their ability to translocate a large number of chemically and structurally unrelated compounds. The most widely investigated prototype is the P-glycoprotein (P-gp or ABC$^{B1}$), which has been widely implicated in conferring multidrug resistance in cancer *(1, 2)*. P-gp is a member of the ATP binding cassette (ABC[1]) superfamily and is known to interact with over 200 drugs. Expression is not confined to malignant tissue since P-gp is also localized in numerous normal tissues associated with excretory or protective roles, including the liver, small intestine, and blood−brain and blood−testes barriers (*3*, *4*). Consequently, the protein plays a major role in determining the pharmacokinetic profile of many clinically used compounds (for review see (*5*)). There is a clear need to develop inhibitors of P-gp in cancer or to modulate its actions in normal tissue, yet only a few highly selective drugs have been developed. Considerable research effort has been directed toward describing the molecular basis of translocation by the protein to enable more rational drug/inhibitor development.

To date, the mechanism of multidrug efflux by P-gp remains poorly understood. Numerous reports demonstrate the presence of multiple drug binding sites for both transported substrates and modulators (*6*−*9*). Their location is within the transmembrane domain (TMD), although the precise spatial orientation of TM segments contributing to the drug binding pocket has not yet been elucidated (*10*−*14*). The translocation process is driven by hydrolysis of ATP at the nucleotide binding domains (NBDs), both of which are required in a functional state to sustain transport activity (*15*−*17*). It is suggested that upon ATP binding the NBDs interact such that nucleotide is coordinated by residues in the Walker-A motif of one NBD and the signature motif of the other NBD (the sandwich dimer). The catalytic cycle is visualized as alternating between NBDs, with the opening of the NBD sandwich dimer thought to be necessary for the release of ADP and Pi. The extent of opening at the NBD/NBD interface may of course be restricted to that just sufficient for ATP binding and ADP release, rather than a complete disengagement. Interestingly, P-gp displays low-level ATP hydrolysis in the absence of drug substrate, so-called basal ATPase activity, which is stimulated several fold in the presence of transported substrates and modulators. The origin of basal ATPase activity remains unexplained. Clearly, the process of drug translocation is a complex multifactorial one (*18*) and requires considerable co-ordination of inter-domain communication. Despite the investigations described above, there is still a paucity of information detailing which regions of the TMDs contain the drug binding sites or which segments of the transporter mediate communication between the drug binding sites and the NBDs.

† This research was funded by a Cancer Research UK Program Grant (SP1861/0401), the Canadian Institutes of Health Research, and Alberta Heritage Foundation for Medical Research.

* To whom correspondence should be addressed. Tel: +44 1865 221 110. Fax: +44 1865 221 834. E-mail: richard.callaghan@ndcls.ox.ac.uk.

‡ University of Oxford.

§ University of Nottingham.

|| University of Calgary.

[1] Abbreviations: ABC, ATP binding cassette transporter; TMD, transmembrane domain; NBD, nucleotide binding domain; DMSO, dimethyl-sulfoxide; DMEM, Dulbecco's Modified Eagle's Medium; ATP, adenosine triphosphate; IAAP, iodo-aryl-azido-prazosin.

10.1021/bi700447p CCC: $37.00 
Published on Web 08/14/2007

Table 1: Mutagenic Oligonucleotide Primers Used to Generate TM6 Mutations[a]

| mutation | primer sequence 5′−3′ | diagnostic restriction digest |
|---|---|---|
| **S344C** | TTAATTGGGGCcTTT**tGT**GTTGGACAG | + Eco 0109 I |
| **V345C** | TTAATTGGGGCaTTcAGT**tgT**GGACAGGCAT | + Bsm I |
| **G346C** | F:GGGGCTTTTAGTGTT**tGc**CAGGCgTCTCCAAGCATTG<br>R:CAATGCTTGGAGAcGCCTGgCaAACACTAAAAGCCCC | +Bsa H I |
| **Q347C** | GCTTTTAGTGTTGGA**tgc**GCATCTCCAAG | + Fsp I |
| **A348C** | GTTGGACAG**tgc**agcCCAAGCATTG | + Bsg I |
| **S349C** | GGACAGGCA**Tgc**CCAAGTATTGAAGCA | + Sph I |
| **A354C** | CAAGCATTGAA**tgc**TTTGCAAATG | + Bsm I |
| **G360C** | CAAATGCAAGA**tGc**GCAGCTTATG | + Fsp I |

[a] Primer sequences contain an introduced cysteine residue (bold) and additional silent mutations (lower case), with respect to the coding sequence that generates, or removes, the indicated restriction site.

The first implication of a specific region in mediating drug−P-gp interaction was obtained in cells selected for resistance to actinomycin D (*19*). These cells displayed a non-conventional pharmacological profile, and isolated P-gp contained mutations within transmembrane segment 6 (TM6), indicating a role in defining substrate specificity. An increasing number of studies indicated that mutations within TM6 produced (i) an altered spectrum of resistance to cytotoxic drugs, (ii) restoration of cellular drug accumulation, and (iii) impaired drug stimulation of ATP hydrolysis by P-gp (*20*−*23*). More recent approaches to elucidate the localization of the drug binding site of P-gp suggest that residues within TM6 in close proximity to TM12 and TM11 form part of a global drug binding pocket (*24*−*26*). The topography of the extracellular section of TM6 has recently been defined (*27*), and the helix is proposed to undergo considerable conformational change in response to events emanating from the nucleotide binding domains. However, a specific role for individual residues within TM6 has been difficult to assign; for example, residue L339 has been reported to make contact with TM12 (*26*), mediate verapamil binding to P-gp (*28*), or facilitate communication to the NBDs (*29*).

Structural investigations of P-gp (*30*−*32*) and the related bacterial transporter Sav1866 (*33*) indicate that TM6 is intimately and directly linked to NBD1 via an α-helical extension of the cytoplasmic portion of TM6. In the present article, we used cysteine-scanning mutagenesis to investigate the contribution of residues in the cytosolic region of TM6 to P-gp function. Our results are consistent with a revised view of the basal ATPase activity of P-gp, in which the rate of ATP hydrolysis in the absence of drug substrate is regulated by residues or regions within the TMDs. More specifically, our data suggest a model in which residue G346 in the cytosolic α-helical section of TM6 is intimately involved in TMD:NBD communication.

## EXPERIMENTAL PROCEDURES

*Materials.* Octyl-β-D-glucoside, C219 antibody, and Ni-NTA His Bind Superflow resin were obtained from Merck Biosciences (Nottingham, UK). The antibodies 4E3 and goat-anti-mouse-RPE were from Dako (Glostrup, Denmark). Dimethyl-sulfoxide (DMSO) disodium adenosine triphosphate ($Na_2ATP$), cholesterol, vinblastine, rhodamine123, and nicardipine were all from Sigma (Poole, UK). Crude *Escherichia coli* lipid extract was obtained from Avanti Polar Lipids (Alabaster, ). Insect-Xpress medium was purchased from Cambrex BioScience (Nottingham, UK) and Excell 405 from AMS Biotechnology (Abingdon, UK). [α-$^{32}$P]-Azido-ATP (430-740GBq/mmol) was purchased from Affinity Labeling Technologies (Lexington, KY, USA), and [$^{125}$I]-iodo-aryl-azido-prazosin (81.4TB q/mmol) was obtained from Perkin-Elmer LAS (Boston, MA, USA). Hoechst33342 was obtained from Invitrogen-Molecular Probes (Paisley, UK).

*Site-Directed Mutagenesis. Introduction of Cysteines.* Mutants were constructed using the Altered sites II (Promega) or the QuickChange (Stratagene) mutagenesis systems with the pAlter-MCHS cDNA template. MCHS is the DNA coding for P-gp devoid of cysteines and containing a C-terminal hexa-histidine tag. The latter was employed to enable subsequent purification, and the template for construction of the cysteine-less isoforms was the wild-type P-gp (*14*, *27*). Endogenous cysteines were mutated to serine in this study rather than the alanine mutation employed elsewhere (*15*−*17*). Mutagenic oligonucleotides were designed containing the bases TGC or TGT, coding for cysteine, and a silent new restriction site (Table 1). Mutants were identified by diagnostic restriction digests, and fragments of the cDNA containing the desired mutation were then sub-cloned into the expression vectors pCIneo_MCHS, pBlueBac4.5_MCHS, and pFastBac1_MCHS to generate the required constructs. The sub-cloned regions were sequenced (Biochemistry, University of Oxford) to ensure the fidelity of the mutagenesis.

*Transient Expression of P-gp in Mammalian HEK293T Cells.* Human Embryonic Kidney 293T cells (HEK293T) were cultured in Dulbecco's Modified Eagle's Medium (DMEM) with 10% (v/v) foetal calf serum (FCS), supplemented with antibiotics (100 U/mL penicillin, 100 μg/mL streptomycin). For transfections, the HEK293T cells were seeded in 35 mm diameter tissue culture dishes at a density of $5 \times 10^5$ cells. Twenty hours later, a mixture of 5 μg of pCIneo derivatives (containing cDNA for P-gp isoforms) and 6.5 μg of polyethyleneimine (PEI) was added to the cells. This transfection medium was added in a solution of DMEM containing 5% FCS and left for a further 24 h. The medium was then replaced with DMEM containing 10% FCS and left for a further 24 h.

For analysis of protein expression, cells were resuspended in lysis buffer (50 mM Tris·HCl at pH 7.4, 150 mM NaCl, 1% (v/v) NP-40, and protease inhibitors), and the solubilized proteins were resolved with SDS−PAGE and P-gp detected with the C219 antibody following immuno-blotting.

*Whole Cell FACS Assay for Rhodamine123 Transport.* Following transfection, cells were harvested and incubated in FACS buffer (FB) comprising phenol red free DMEM containing 1% (v/v) FCS. The suspension was supplemented with 2 $\mu$M rhodamine123 and 1.7 $\mu$g/mL of the anti-P-gp antibody 4E3, which recognizes an extracellular epitope. The mixture was incubated for 1 h at 37 °C and the cells then washed with FB. The cells were subsequently incubated with 5 $\mu$g/mL goat-anti-mouse secondary antibody conjugated with R-phycoerythrin (RPE) in FB for 50 min at 4 °C. Cells were washed and resuspended in FB containing 5 $\mu$g/mL propidium iodide (PI). The fluorescence associated with cells was measured with a FACSCalibur flow cytometer using 488 nm argon laser excitation. The detection filters were set at 530 nm (rhodamine 123), 585 nm (RPE), and 661 nm (PI). The percentage of P-gp-expressing cells able to transport rhodamine123 was calculated as previously described (*34*). Briefly, the following formula was used to calculate the percentage of P-gp-expressing cells able to transport R123:

$$\textit{Transport activity} = \frac{\text{cells in lower right quandrant}}{\text{cells in the lower and upper right quadrants}} \times 100\%$$

*Generation of Recombinant Baculovirus.* Recombinant baculovirus was generated with either (i) the Bac-N-Blue or (ii) the Bac-to-Bac baculovirus expression systems (Invitrogen). Mutants (G346C, Q347C, A348C, S349C, A354C, and G360C) in pBlueBac_4.5 (2 $\mu$g) were cotransfected into *Spodoptera frugiperda* (Sf9) cells with Bac-N-Blue DNA (0.25 $\mu$g) and *Cellfectin* (10 $\mu$g) in medium without FCS and antibiotics. Baculovirus was harvested by centrifugation of the cells after 3 days, and the recombinant baculovirus expressing the mutant P-gp was isolated as described by the manufacturer. Alternatively, mutant isoforms (S344C and V345C) in pFastBac-1 were transformed into DH10Bac *E. coli*. The bacmid DNA was isolated and P-gp cDNA incorporation verified by PCR. Transfection into Sf9 cells was achieved with Bacmid DNA (3 $\mu$g) and *Cellfectin* Reagent (6 $\mu$g) in medium without FCS or antibiotics. The recombinant baculovirus was collected after 4 days of infection.

*Expression, Purification, and Reconstitution of P-gp.* *Trichplusia ni* (High-five) cells were infected with recombinant baculovirus containing mutant isoforms of P-gp and harvested 3 days post-infection by centrifugation. Membranes were isolated as previously described (*14*, *27*) and stored at −80 °C for up to 1 year. Purification by immobilized metal affinity chromatography and reconstitution of each isoform of P-gp were achieved using procedures previously described in full (*14*, *27*). Confirmation of reconstitution was achieved via analysis of lipid and protein migration through sucrose density gradients. Protein concentration following reconstitution was determined using densitometric analysis of SDS−PAGE gels stained with Coomassie-Brilliant Blue, with bovine serum albumin as a standard (*14*, *27*). The efficiency of reconstitution was further examined by dynamic light scattering because of its sensitivity to particle size and polydispersity. Approximately 500 ng of purified, reconstituted cysteine-less P-gp was appropriately diluted with buffer (150 mM NaCl, 20 mM Tris, 1.5 mM $MgCl_2$, and 20% glycerol at pH 6.8), placed in a quartz cuvette, and the absorbance measured using the Protein Solutions DynaPro spectrophotometer (Protein Solutions Inc.). The hydrodynamic radius was calculated using the software program Dyna Pro (Proterion, Piscataway, NJ).

*ATPase Activity of Purified P-gp.* The ATP hydrolytic activity of purified, reconstituted P-gp was determined by measuring the release of inorganic phosphate using modifications (*14*, *27*) of a colorimetric assay (*35*). Michaelis−Menten parameters were determined by incubating proteoliposomes with varying concentrations of MgATP in the presence or absence of nicardipine or vinblastine (30 $\mu$M). To determine the potency of drugs to stimulate or inhibit ATP hydrolysis, the proteoliposomes were incubated in MgATP (2 mM) with varying drug concentrations.

*[$\gamma^{32}$P]-8-Azido-ATP Binding to P-gp.* Nucleotide binding to P-gp was assessed by photoactive labeling of purified, reconstituted protein with [$\gamma$-$^{32}$P]-8-azido-ATP, as previously described (*36*). Proteoliposomes (0.2 $\mu$g) were incubated with concentrations up to 100 $\mu$M [$\gamma$-$^{32}$P]-8-azido-ATP in a total volume of 20 $\mu$L on ice for 12 min under subdued lighting and then subjected to UV-irradiation (100 W, 5 cm, $\lambda$ = 265 nm) for 8 min. Post-irradiation, the samples were resolved with 7.5% (v/v) SDS−PAGE and labeling detected by autoradiography. The interaction of ATP with the protein was determined with 100 $\mu$M [$\gamma$-$^{32}$P]-azido-ATP in the presence of increasing concentrations of nucleotide (0.01-2 mM). The interaction with ADP was determined using 10 $\mu$M [$\gamma$-$^{32}$P]-azido-ATP in the presence of 0.03−1 mM ADP.

*[$^{125}$I]-Iodo-aryl-azido-prazosin Binding to P-gp.* The drug−P-gp interaction was assessed by measuring the binding of the photoactivateable modulator [$^{125}$I]-iodo-aryl-azido-prazosin (IAAP). Proteoliposomes (0.25 $\mu$g) were incubated in the presence of 10 nM [$^{125}$I]-IAAP in a total volume of 30 $\mu$L in the presence or absence of nicardipine (30 $\mu$M), vinblastine (100 $\mu$M), rhodamine123 (100 $\mu$M), or Hoechst33342 (100 $\mu$M). The proteoliposomes and drugs were incubated for 2 h at 20 °C in the dark to reach equilibrium. The samples were then placed on ice for 10 min and subsequently irradiated with UV light ($\lambda$ = 265 nm, 100 W, 5 cm) for 8 min, and the protein was resolved with 7.5% (v/v) SDS−PAGE. The gels were washed extensively with distilled water, fixed in 10% (v/v) acetic acid and 25% (v/v) isopropanol, and dried prior to autoradiography with Kodak Biomax Film.

*Statistical Analysis.* All data manipulation and statistical analysis were performed using GraphPad Prism version 4. Comparisons of data sets for mutant isoforms were performed using analysis of variance (ANOVA), applying Newman−Keuls post-hoc test, where significant ($P < 0.05$) differences were found between mean values.

*Homology Modeling of P-Glycoprotein.* The structure of Sav1866, imaged in the ADP-bound state and resolved to 3.0 Å (*33*), was used as the template structure for homology models of the N-terminal and C-terminal halves of human P-gp (NCBI AAA59575). Two copies of Sav1866 (PDB code 2HYD) were aligned with the P-gp sequence (*37*, *38*). The alignment was checked using secondary structure predictions (*39*). Each half of P-gp was modeled separately using Modeller (*40*). The N- and C-terminal models were dimerized, refined, and energy minimized to remove any residue clashes. The native P-gp model underwent an *in silico* G346C mutation and was further energy minimized to refine

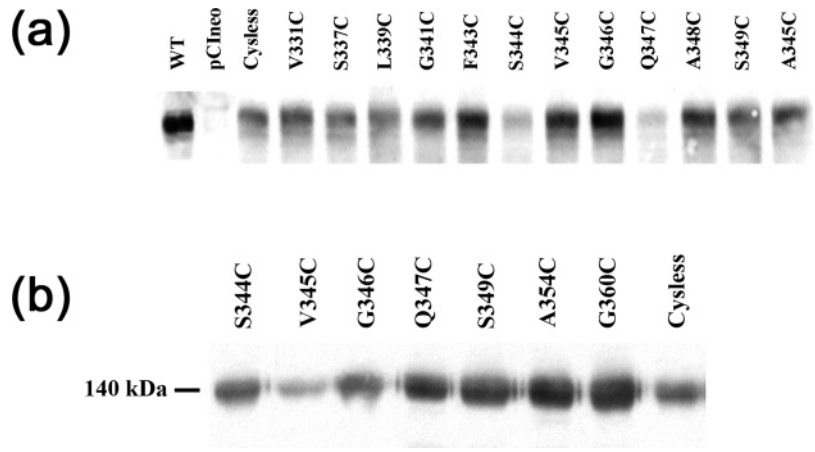


FIGURE 1: Expression of P-gp in HEK293T and High-5 cells. A representative example of the expression of P-gp isoforms obtained from whole cell lysates of (a) HEK293T and (b) High-five cells. P-gp expression was detected using western immuno-blotting with the anti-P-gp monoclonal antibody C219. Proteins were separated using 8% SDS−PAGE, and the amount of protein loaded into each lane corresponds to 20 $\mu$g of total protein in the lysate. The pCIneo lane did not contain cDNA for P-gp.

the structure. The quality of the native P-gp and G346C mutant P-gp models was assessed using PROCHECK (*41*) and WHATIF (*42*).

## RESULTS

*Expression of Mutant P-gp Isoforms in HEK293T and High-Five cells.* Mutant P-gp isoforms were initially expressed in HEK293T cells to provide a rapid initial screen for major functional perturbation and in insect cells for more detailed biochemical investigations on pure protein. For comparison, we also examined the expression and transport function of protein with mutated residues in the upper half of TM6. Both the expression level and the overall protein function of these mutants were indistinguishable from those in the cytosolic half of TM6. Figure 1 shows that full length protein for each of the isoforms was produced in both the HEK293T cells following transient transfection and insect cells following infection with recombinant baculovirus. Figure 1 is a representative gel and transient transfections are associated with some degree of variability. There were no mutant isoforms with a consistently different level of expression. Moreover, there was no evidence of lower molecular weight species corresponding to mis-processed (i.e., not fully glycosylated) P-gp.

*Overall Functional Assessment in HEK293T Cells.* Rhodamine123 accumulation was measured for each of the TM6 mutants, cysteine-less and wild-type P-gp, and summarized in Figure 2. Steady-state accumulation of the fluorescent dye rhodamine123 was used to measure the transport activity of the various P-gp isoforms. The two-color flow cytometry assay detects transfected cells with the P-gp antibody 4E3, which is subsequently detected by a fluorescent secondary antibody, and the accumulation of rhodamine123 (*34*). The epitope of 4E3 is externally localized, and the signal is therefore related to protein in the plasma membrane only. Cells expressing functional P-gp have a low rhodamine123 signal due to transport. Addition of the P-gp modulator XR9576 increased the accumulation of rhodamine123 compared to that in untransfected cells, indicating the transport of rhodamine123 solely by P-gp (Figure 2a). In addition, the data obtained for G346C displayed a shift from the lower right quadrant toward the upper right quadrant. This is indicative of reduced rhodamine123 transport, despite the expression and correct trafficking of P-gp. The relative expression levels for the various mutants did not show any consistent trend; for example, the dot plot on Figure 2a suggests higher expression of cysteine-less protein, compared to G346C protein whereas the immuno-blot in Figure 1a indicates the opposite. The cysteine-less isoform provides the template for the introduction of mutations, and Figure 2b clearly demonstrates that the activity was identical to that of wild-type P-gp. All of the isoforms of P-gp were capable of significant rhodamine123 transport, indicating that the introduction of a cysteine residue did not cause major functional perturbation and hence has not affected the structural integrity of P-gp. The striking observation from the data in Figure 2b was that only one of the mutations caused a significant reduction in the transport function of P-gp, namely, isoform G346C. This assay is, however, merely a reflection of overall protein function and is not a sophisticated discriminator of kinetic differences between protein isoforms. To achieve the latter objective required purification of the mutants. Previous studies (*14*, *27*) demonstrated that the cysteine-less and wild-type P-gp isoforms are not functionally distinct on the basis of ATPase activity and substrate binding properties. Consequently, the former is used as the reference point within the manuscript, particularly as all of the single cysteine insertions are based upon this template.

*Purification of P-gp Isoforms. Characteristics of ATP Hydrolysis.* The efficient solubilization and purification of P-gp from High-Five cell membranes has previously been characterized (*14*, *27*), and the final product displayed approximately 90% purity and a yield of 0.5−1.0 mg per liter of insect cell culture. Figure 3a shows the purity of P-gp following immobilized metal affinity chromatography, with greater than 90% eluting at 120 mM imidazole and minimal loss of P-gp at early stages of the procedure. The success of reconstitution was defined as the comigration of lipid ([$^3$H]-PC) and P-gp through a sucrose density gradient. Sucrose density centrifugation was routinely performed for each purification preparation, and reconstitution efficiency did not vary between the mutant isoforms. The protein was shown to be efficiently reconstituted into liposomes as demonstrated

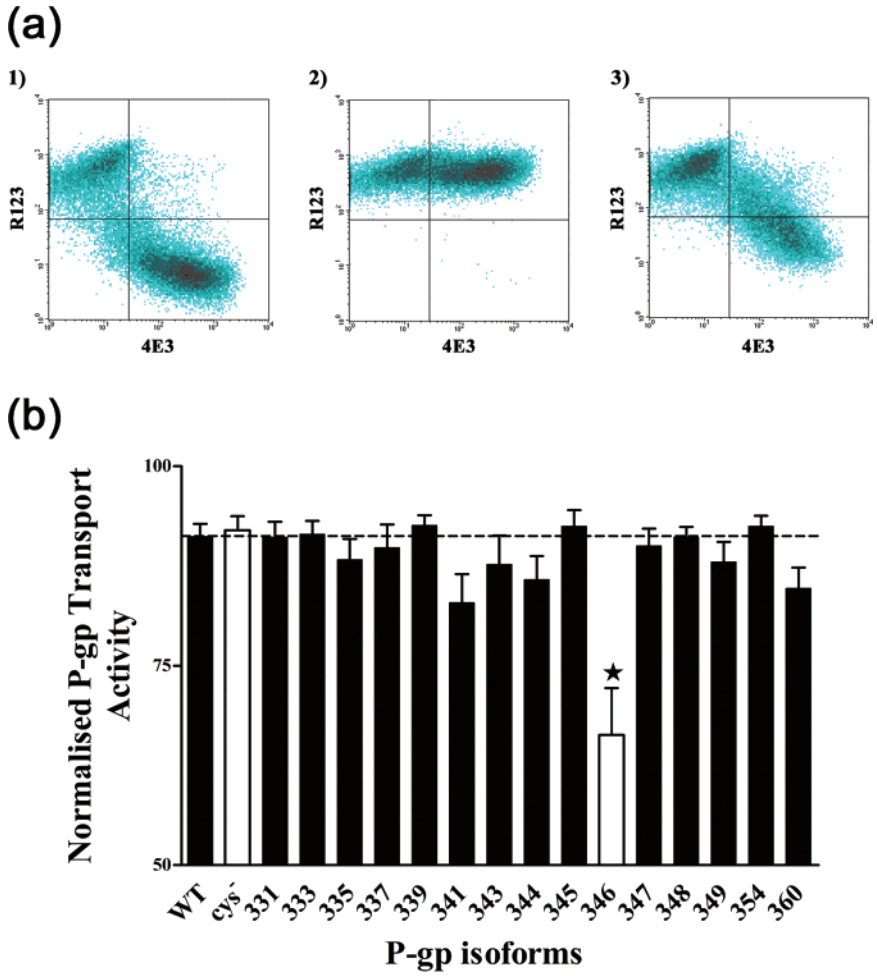


FIGURE 2: Transport of rhodamine123 by mutant P-gp isoforms in HEK293T cells. (a) Quadrant analysis for the cysteine-less and G346C isoforms obtained from the flow cytometry assay. The panels depict the correlation between rhodamine123 accumulation (*y*-axis) and P-gp expression, as detected by 4E3 fluorescence (*x*-axis). The panels show dot-plots of single cells and are divided into four quadrants. The lower-right quadrant represents P-gp-expressing cells capable of rhodamine123 extrusion. Panels 1 and 2 were obtained for the cysteine-less isoform in the absence or presence of the P-gp inhibitor XR9576 (10 $\mu$M), respectively. Panel 3 was obtained for the G346C isoform in the absence of inhibitor. (b) Histogram showing the relative ability of wild-type, cysteine-less, and TM6 mutant P-gp isoforms to transport rhodamine123. An analysis of transport activity was done by flow cytometry, and the values were normalized for protein expression (i.e., 4E3 reactivity) as described in Experimental Procedures. The *y*-axis indicates the percentage of P-gp-expressing cells that were capable of mediating rhodamine123 efflux. The values are expressed as mean ± SEM from at least six independent observations. The asterisk indicates a statistically significant difference from the value obtained for cysteine-less P-gp.

in Figure 3b. The use of detergent adsorption onto SM2-Biobeads ensures the complete removal of surfactant. Moreover, the homogeneity of the samples was confirmed by the presence of protein and lipid in a single fraction in the sucrose gradient, and there was no dispersity in either. This was confirmed by the data in Figure 3c obtained with dynamic light scattering (DLS). DLS provides a reliable estimate of the homogeneity in particle sizes as revealed in the distribution profile in the histogram for cysteine-less P-gp. The estimated size (hydrodynamic radius) of proteoliposomes from the DLS analysis was 202 ± 12 nm. There were no significant differences in the hydrodynamic radii of proteoliposomes produced for any mutant isoforms of the protein. The lipid composition of the proteoliposomes does produce leaky liposomes, despite the presence of cholesterol (*43*). These techniques demonstrate the homogeneity of the proteoliposomes; however, they do not provide a morphological characterization. Because the subsequent characterizations do not include transport measurements, there is no concern with precise morphology of the vesicles.

Figure 4 demonstrates a representative curve for the ATPase activity of purified cysteine-less P-gp and the G346C isoform in the absence or presence of the modulator nicardipine (30 $\mu$M). The ATPase activity displayed Michaelis−Menten properties, and the presence of nicardipine increased the maximal rate of hydrolysis. Cysteine-less P-gp was characterized by a basal $V_{max}$ of 0.48 ± 0.10 $\mu$mol min$^{-1}$ mg$^{-1}$ and a $K_m$ of 0.54 ± 0.05 mM. The $V_{max}$ was increased by nicardipine to 1.37 ± 0.19 $\mu$mol min$^{-1}$ mg$^{-1}$, while vinblastine produced a comparatively smaller stimulation in $V_{max}$ of 0.98 ± 0.10 $\mu$mol min$^{-1}$ mg$^{-1}$. Drug stimulation did not significantly affect the $K_m$ for ATP hydrolysis.

Data similar to that determined in Figure 4 was determined for each of the mutant TM6 isoforms in the presence or absence of the substrates vinblastine or nicardipine, and the averaged results from multiple preparations are summarized in Table 2. The most dramatic effects on ATPase activity were observed with the G346C isoform (bold, italic text), which is consistent with the altered rhodamine123 transport data (Figure 2). The basal ATPase activity was reduced

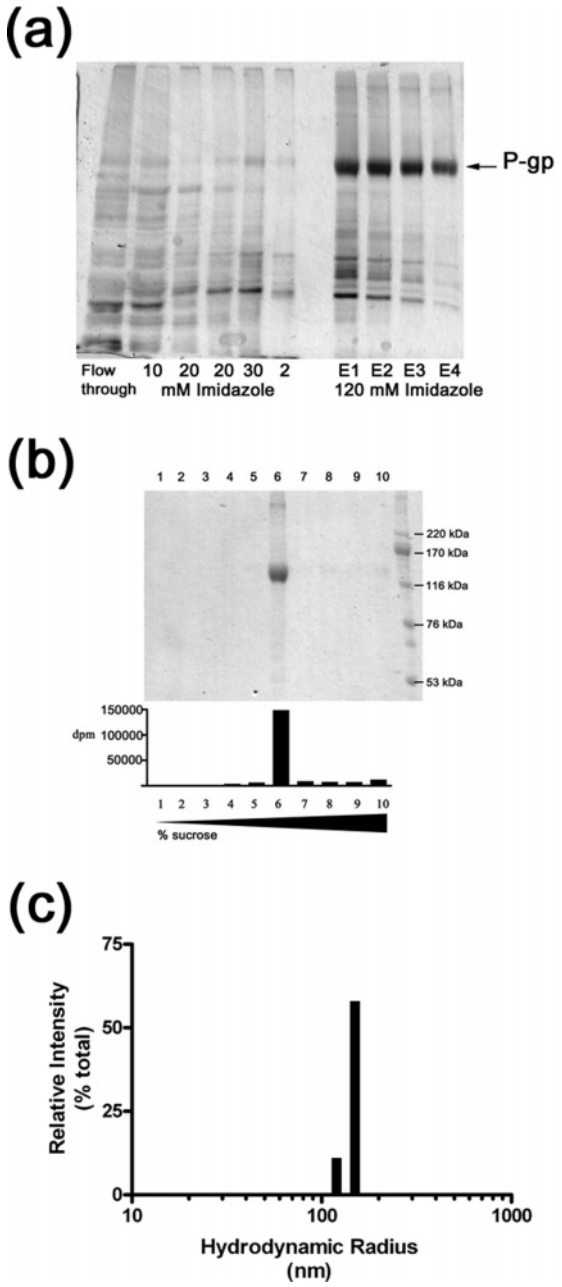


FIGURE 3: Purification and reconstitution of P-gp Isoforms. (a) All P-gp isoforms were solubilized from High-five membranes in 2% (w/v) octyl-glucoside and purified by immobilized metal affinity chromatography. The SDS−PAGE gel (8%) was silver-stained and demonstrates the retention of P-gp (G346C) on the column through the washing steps (up to 30 mM imidazole) and its elution in 120 mM imidazole. The arrow corresponds to the migration of P-gp at 140 kDa. (b) Following reconstitution, an aliquot of P-gp (G346C) was subjected to sucrose density centrifugation. Ten fractions were collected from the gradient and P-gp distribution demonstrated by SDS−PAGE (8%) with Coomassie-Brilliant Blue staining. An aliquot of each fraction was assessed for the presence of the marker lipid [$^3$H]-PC (dpm) using liquid scintillation counting. (c) Reconstituted P-gp samples were examined by dynamic light scattering to assess the homogeneity and size of proteoliposomes generated. The histogram provided is a representative example taken for the cysteine-less isoform of the protein.

approximately 9-fold to 0.056 ± 0.007 $\mu$mol min$^{-1}$ mg$^{-1}$ by the G346C mutation. A similar reduction was observed for the maximal rate of ATP hydrolysis in the presence of nicardipine; however, the degree of stimulation (3.4-fold) by this compound remained almost identical to that observed

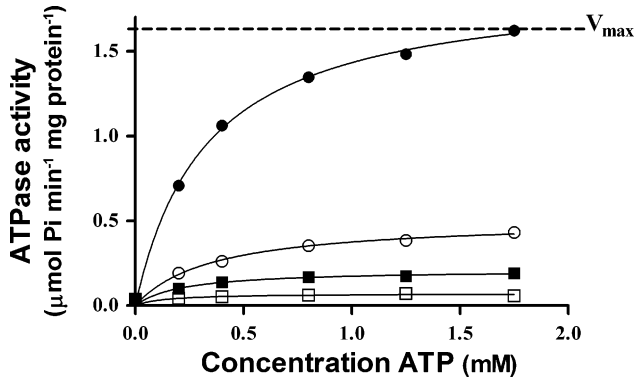


FIGURE 4: ATPase activity of purified, reconstituted cysteine-less and G346C isoforms of P-gp. ATPase activity was determined as a function of ATP concentration for cysteine-less P-gp (○, ●) and the G346C mutant (□, ■) in the absence (open symbols) or presence (closed symbols) of 30 $\mu$M nicardipine. The graph is a representative example from a single experiment. ATP hydrolysis was measured by the liberation of inorganic phosphate using a colorimetric assay as described in Experimental Procedures. Each point contained 0.2 $\mu$g of purified, reconstituted P-gp, and the assay was performed at 37 °C for 20 min. The relationships between activity and ATP concentration were fitted with the Michaelis−Menten equation by nonlinear least-squares regression.

with the cysteine-less isoform (Figure 4). In contrast, unlike the control cysteine-less P-gp, the ATPase activity of the G346C mutant was not stimulated by the presence of 30 $\mu$M vinblastine.

The other mutant TM6 isoforms did not display any significant change in basal ATPase activity, while the drug-stimulated ATPase activity was affected in some isoforms. The $V_{max}$ in the presence of nicardipine was also reduced for Q347C but increased for the A348C and A354C isoforms. A348C also showed increased $V_{max}$ in the presence of vinblastine, but the overall fold stimulation for both substrates was comparable to that of cysteine-less P-gp. Overall, the $K_m$ of ATP was not changed for most P-gp isoforms, but for G346C and Q347C, it was reduced in the basal state when compared to that of cysteine-less P-gp. For Q347C, the $K_m$ remained lower in the presence of nicardipine, and in the presence of both nicardipine and vinblastine, the $K_m$ value was higher for A354C.

The above data on drug stimulation of ATPase activity were obtained from Michaelis−Menten characterization but only at a single drug concentration. Consequently, full dose−response analyses to determine the potencies of drug stimulation of ATP hydrolysis were undertaken. The results are summarized in Table 3. Nicardipine stimulated the ATPase activity of all of the mutants, but the degree of stimulation was significantly different from that produced in cysteine-less P-gp for some of the isoforms. It was increased for S344C, A354C, and G360C, and decreased for Q347C, but the potency of stimulation was unchanged compared to that of cysteine-less P-gp. These results confirm that the interaction of nicardipine with the mutant TM6 isoforms of P-gp is preserved following the introduction of cysteine residues and that this region may not be involved in mediating the binding of this potent modulator. In contrast, mutations G346C, Q347C, and S349C abrogated the stimulation of ATP hydrolysis by vinblastine. Although, the degree of stimulation observed with vinblastine in other mutant

Table 2: Michaelis−Menten Parameters for ATPase Activity of P-gp[a]

| | basal | | nicardipine | | vinblastine | |
|---|---|---|---|---|---|---|
| | $V_{max}$ ($\mu$mol/min/mg) | $K_m$ (mM) | $V_{max}$ ($\mu$mol/min/mg) | $K_m$ (mM) | $V_{max}$ ($\mu$mol/min/mg) | $K_m$ (mM) |
| **CYS$^-$** | 0.48 ± 0.10 | 0.54 ± 0.05 | 1.37 ± 0.19 | 0.38 ± 0.03 | 0.98 ± 0.10 | 0.38 ± 0.02 |
| **S344C** | 0.30 ± 0.05 | 0.34 ± 0.05 | 1.71 ± 0.28 | 0.45 ± 0.07 | 0.84 ± 0.09 | 0.28 ± 0.03 |
| **V345C** | 0.43 ± 0.07 | 0.42 ± 0.06 | 1.69 ± 0.29 | 0.24 ± 0.01 | 0.82 ± 0.15 | 0.36 ± 0.04 |
| ***G346C*** | *0.06 ± 0.01** | *0.21 ± 0.05** | *0.15 ± 0.02** | *0.24 ± 0.05* | *0.06 ± 0.02** | *0.26 ± 0.09* |
| ***Q347C*** | *0.25 ± 0.03* | *0.21 ± 0.03** | *0.47 ± 0.06** | *0.13 ± 0.01** | *0.39 ± 0.13* | *0.19 ± 0.02* |
| **A348C** | 0.79 ± 0.15 | 0.37 ± 0.03 | 2.90 ± 0.52* | 0.40 ± 0.05 | 1.58 ± 0.30* | 0.41 ± 0.06 |
| **S349C** | 0.38 ± 0.04 | 0.36 ± 0.06 | 1.00 ± 0.10 | 0.23 ± 0.03 | 0.45 ± 0.04 | 0.27 ± 0.03 |
| **A354C** | 0.47 ± 0.10 | 0.50 ± 0.10 | 2.21 ± 0.37* | 0.59 ± 0.08* | 1.29 ± 0.23 | 0.61 ± 0.15* |
| **G360C** | 0.35 ± 0.03 | 0.36 ± 0.02 | 1.88 ± 0.12 | 0.46 ± 0.08 | 1.00 ± 0.07 | 0.43 ± 0.02 |

[a] ATPase activity was plotted as a function of ATP concentration and the $V_{max}$ and $K_m$ parameters obtained by nonlinear regression of the Michaelis−Menten equation. The values are the mean ± SEM of at least four independent preparations, and * refers to a significant difference ($P < 0.05$) compared to the cysteine-less (CYS$^-$) isoform.

Table 3: Potency and Degree of Drug Stimulation of ATP Hydrolysis by P-gp[a]

| | nicardipine | | vinblastine | |
|---|---|---|---|---|
| | $EC_{50}$ ($\mu$M) | fold-stimulation | $EC_{50}$ ($\mu$M) | fold-stimulation |
| **CYS$^-$** | 3.2 ± 0.3 | 3.4 ± 0.3 | 4.2 ± 0.7 | 2.4 ± 0.2 |
| **S344C** | 5.4 ± 0.3 | 5.9 ± 0.4* | 12.2 ± 0.5* | 2.9 ± 0.2 |
| **V345C** | 3.2 ± 0.1 | 3.9 ± 0.1 | 9.3 ± 1.1* | 2.1 ± 0.1 |
| ***G346C*** | *5.5 ± 1.1* | *3.4 ± 0.3* | *ND* | *1.0 ± 0.1** |
| ***Q347C*** | *2.0 ± 0.6* | *2.0 ± 0.1** | *ND* | *1.3 ± 0.1** |
| **A348C** | 3.4 ± 0.4 | 3.9 ± 0.3 | 9.0 ± 2.1* | 2.3 ± 0.2 |
| ***S349C*** | *2.3 ± 0.1* | *2.6 ± 0.1* | *ND* | *1.2 ± 0.1** |
| **A354C** | 3.5 ± 0.2 | 5.0 ± 0.3* | 6.6 ± 0.5 | 2.5 ± 0.2 |
| **G360C** | 4.8 ± 0.5 | 5.5 ± 0.3* | 5.9 ± 0.4 | 2.7 ± 0.1 |

[a] ATPase activity was plotted as a function of drug concentration and the potency and degree of stimulation obtained by nonlinear regression of the dose−response relationship equation. The values are the mean ± SEM of at least four independent preparations, * refers to a significant difference ($P < 0.05$) compared to the cysteine-less (CYS$^-$) isoform, and ND corresponds to not detected.

isoforms (2.1−2.9-fold) was similar to that seen in cysteine-less P-gp (2.4 ± 0.2-fold), the potency was generally reduced.

In summary, specific mutations within the cytosolic region of TM6 appear to modulate ATPase activity, even in the absence of drug. Moreover, the mutations impact differently on the ability of nicardipine and vinblastine to stimulate ATPase activity with the efficacy of the latter abrogated. The altered potency or extent of effect may be attributed to impaired binding of vinblastine to the mutant isoforms or modified communication of TM6 to the NBDs.

*[$^{125}$I]-IAAP Binding to TM6 Mutated Isoforms of P-gp.* A photoaffinity labeling approach was utilized to ascertain whether the mutations altered the fidelity of drug binding to the TM6 isoforms. Figure 5 provides representative autoradiograms for the specific photolabeling of the substrate [$^{125}$I]-IAAP to the cysteine-less and A348C isoforms of P-gp. The autoradiogram demonstrates that the binding to P-gp was displaceable by nicardipine, vinblastine, and Hoechst33342, while rhodamine123 produced a moderate increase in labeling. The degree of displacement by each drug in the series of TM6 mutants was quantified by densitometry (Table 4). Nicardipine, vinblastine, and Hoechst33342 all produced significant, specific displacement of [$^{125}$I]-IAAP photolabeling, although a residual fraction remained in each case. Table 4 demonstrates that the fraction of [$^{125}$I]-IAAP displaced by nicardipine, vinblastine, and Hoechst33342 was identical

Table 4: Displacement of [$^{125}$I]-Iodo-aryl-azido-prazosin Binding to P-gp Isoforms[a]

| mutant | nicardipine (30 $\mu$M) | vinblastine (100 $\mu$M) | rhodamine123 (100 $\mu$M) | hoechst33342 (100 $\mu$M) |
|---|---|---|---|---|
| **CYS$^-$** | 0.36 ± 0.06 | 0.38 ± 0.06 | 1.29 ± 0.34 | 0.27 ± 0.05 |
| **S344C** | 0.48 ± 0.03 | 0.40 ± 0.02 | 1.61 ± 0.47 | 0.12 ± 0.01 |
| **G346C** | 0.41 ± 0.06 | 0.30 ± 0.03 | 1.54 ± 0.29 | 0.16 ± 0.05 |
| **Q347C** | 0.56 ± 0.10 | 0.45 ± 0.10 | 1.27 ± 0.16 | 0.16 ± 0.09 |
| **A348C** | 0.40 ± 0.03 | 0.36 ± 0.06 | 1.25 ± 0.18 | 0.20 ± 0.04 |
| **S349C** | 0.39 ± 0.05 | 0.34 ± 0.05 | 2.18 ± 0.62 | 0.31 ± 0.13 |
| **A354C** | 0.43 ± 0.04 | 0.39 ± 0.07 | 1.39 ± 0.25 | 0.21 ± 0.06 |
| **G360C** | 0.52 ± 0.12 | 0.34 ± 0.01 | 1.40 ± 1.37 | 0.23 ± 0.10 |

[a] The fraction of [$^{125}$I]-IAAP labeled P-gp isoforms was determined in the presence of drug and was expressed as a proportion of the amount in the absence of drug. The values represent the mean ± SEM of at least three independent observations.

regardless of the specific isoform. Moreover, vinblastine retained the ability to displace [$^{125}$I]-IAAP binding, demonstrating that it is capable of interacting with P-gp. Consequently, the lack of any effect of vinblastine on ATPase activity in Q347C, S349C, and in particular G346C (Tables 2 and 3) is not due to major disruption of the drug binding site for this substrate by the TM6 mutation.

*Nucleotide Binding Characteristics of G346C.* ATPase activity is a multistep process involving ATP binding, the hydrolytic reaction, and the release of reaction products. To further examine the impact of the G346C mutation on P-gp function, the binding of nucleotide was examined using the photoactive ATP analogue, [$\gamma$-$^{32}$P]-8-azido-ATP. Figure 6a demonstrates the dose-dependent binding of [$\gamma$-$^{32}$P]-8-azido-ATP to the cysteine-less and G346C isoforms of P-gp.

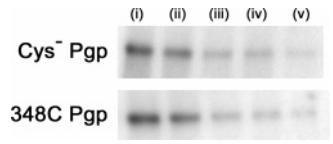


FIGURE 5: [$^{125}$I]-IAAP binding properties of purified, reconstituted mutant P-gp isoforms. The binding of [$^{125}$I]-IAAP was measured by autoradiography of photoaffinity labeled purified, reconstituted cysteine-less and A348C isoforms of P-gp in the presence or absence of various drug substrates (100 $\mu$M). The amount of protein in each reaction was 0.25 $\mu$g, and incubation was in the dark at 20 °C for 2 h. Following incubation, the protein was irradiated as described in Experimental Procedures. The entire reaction volume was analyzed using SDS−PAGE. Lane assignments are as follows: (i) rhodamine123, (ii) no drug, (iii) nicardipine, (iv) vinblastine, and (v) Hoechst33342.

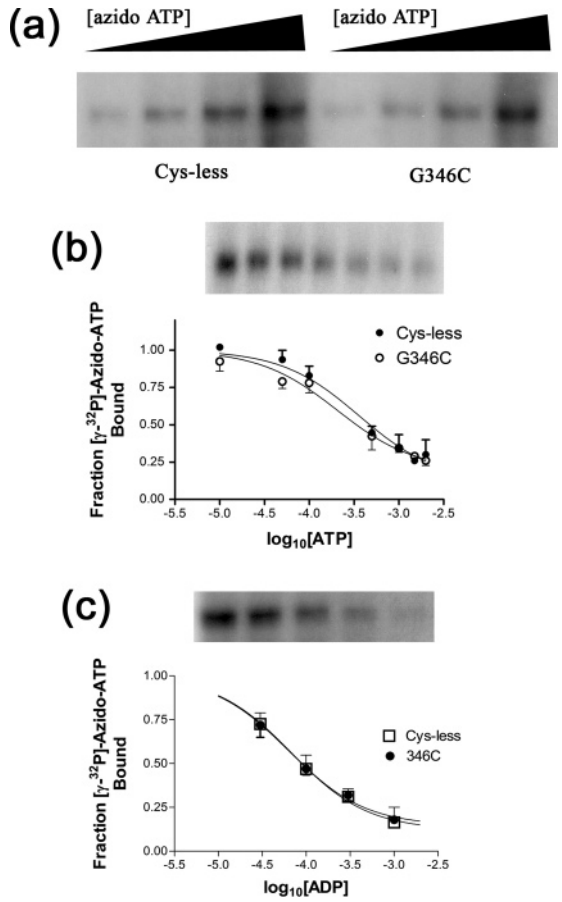


FIGURE 6: Nucleotide binding properties of purified, reconstituted cysteine-less and G346C P-gp. (a) The autoradiogram shows the amount of [$\gamma$-$^{32}$P]-8-azido-ATP bound to purified, reconstituted cysteine-less and G346C isoforms of P-gp. The binding was performed using a concentration of [$\gamma$-$^{32}$P]-azido-ATP that varied between 10 and 100 $\mu$M. Protein was resolved using SDS−PAGE and the amount of labeling detected by autoradiography. (b) Purified, reconstituted cysteine-less and G346C isoforms of P-gp were labeled with [$\gamma$-$^{32}$P]-8-azido-ATP (100 $\mu$M) in the presence or absence of varying concentrations of ATP. The inset to the panel shows a representative autoradiogram for cysteine-less P-gp highlighting the relative labeling at each ATP concentration. The autoradiograms were quantitatively analyzed by densitometry, and the amount of labeling was plotted as a function of ATP concentration. (c) Purified, reconstituted cysteine-less and G346C isoforms of P-gp were labeled with [$\gamma$-$^{32}$P]-8-azido-ATP (10 $\mu$M) in the presence or absence of varying concentrations of ADP. The inset to the panel shows a representative autoradiogram for cysteine-less P-gp and the relative labeling at each ADP concentration. The autoradiograms were quantitatively analyzed by densitometry, and the amount of labeling was plotted as a function of ATP concentration. The amount of protein in each reaction was 0.25 $\mu$g, and incubation was done in the dark at 4 °C for 12 min. Following incubation, the protein was irradiated and analyzed as described in Experimental Procedures. The relationships between photolabeling and ATP or ADP concentrations were analyzed by nonlinear regression using the general dose−response curve. The values are mean ± SEM obtained from three independent observations for (b) and (c).

Langmuir binding analysis was not performed because of the inability to saturate binding with the low concentrations of commercial [$\gamma$-$^{32}$P]-8-azido-ATP. However, the results do indicate that at a concentration of 100 $\mu$M, there was no discernible difference in the binding of the ATP analogue to cysteine-less and G346C isoforms of P-gp.

To confirm that the binding of nucleotide was unaffected by the G346C mutation, the ability of ATP to displace [$\gamma$-$^{32}$P]-8-azido-ATP (100 $\mu$M) photolabeling was assessed. Figure 6b shows a representative autoradiogram for the dose-dependent displacement of [$\gamma$-$^{32}$P]-8-azido-ATP binding by ATP for G346C. The potency of displacement by ATP for the control cysteine-less isoform ($IC_{50}$ = 0.37 ± 0.03 mM) was not significantly different from that observed with the G346C ($IC_{50}$ = 0.21 ± 0.12 mM) isoform, suggesting that the affinity for ATP binding is likely to be similar.

The release of ADP occurs at a late stage of the catalytic cycle and has also been purported to play a role in dictating the overall rate of hydrolysis. The low affinity of ADP binding to ABC transporters precludes its direct measurement. To overcome this problem, the ability to displace ATP binding was used as a measure of the affinity of ADP. An increase in the potency of displacement of [$\gamma$-$^{32}$P]-8-azido-ATP binding by ADP in G346C would signify greater affinity of the dinucleotide, thereby suggesting a slower rate of release. Figure 6c demonstrates that the ADP-mediated displacement of [$\gamma$-$^{32}$P]-8-azido-ATP binding displayed similar potencies for the cysteine-less ($IC_{50}$ = 67 ± 16 $\mu$M) and G346C ($IC_{50}$ = 72 ± 12 $\mu$M) isoforms of the protein.

In summary, the impaired drug transport rate displayed by the G346C mutant isoform of P-gp is characterized by a reduced basal ATPase activity and an altered communication between the TMDs and NBDs subsequent to vinblastine, but not nicardipine, binding. The precise nature of this reduction in ATPase activity is not due to changes in the binding of ATP, the release of ADP, or of the ability of drugs to bind.

*Homology Modeling of TM6 in P-gp Suggests that G346C Disrupts the TMD* α*-Helical Packing.* To provide a possible structural explanation for the unexpected functional effects of the G346C mutation, we have analyzed the native and G346C P-gp homology models, which map over 90% of the P-gp primary sequence, including TM6 in its entirety and the TMD−NBD and NBD−NBD interfaces. The quality of the P-gp homology models was assessed using PROCHECK and WHATIF (*41*, *42*) and found to be of comparable quality to the Sav1866 template. The backbone root-mean-square deviation (RMSD) between Sav1866 and the native and G346C P-gp models was 0.98 Å, while the RMSD between the two P-gp homology models was <0.01 Å, indicating that the backbone conformations are highly similar.

Figure 7a shows that there is a significant bend in the modeled TM6 helix. Analysis of the hydrogen-bonding pattern shows that the normal α-helical bonding pattern is disrupted between residues T333−I340 and V345−P350, pinpointing these amino acids as key regions in TM6 α-helix deformation. The first of these regions, T333−I340, consists primarily of adjacent $\beta$-branched and aromatic residues and terminates with a valine−leucine−isoleucine motif (residues 338−340). Previous analysis of comparable sequences suggests that this arrangement of $\beta$-branched amino acids destabilizes α-helices (*44*), in agreement with our model. Because of this distortion of TM6, the side chain of Leu339 has a high surface accessibility, which is consistent with previous experimental labeling results (*29*). Heuristic calculations on the intracellular portion of TM6 suggest that it acts as a lever through which conformational changes are communicated to the NBD. The introduction of an *in silico* G346C mutation in the P-gp homology model shows that the 346C side chain adopts an energetically favorable conformation when it is coordinated by A342 (TM6), F303,

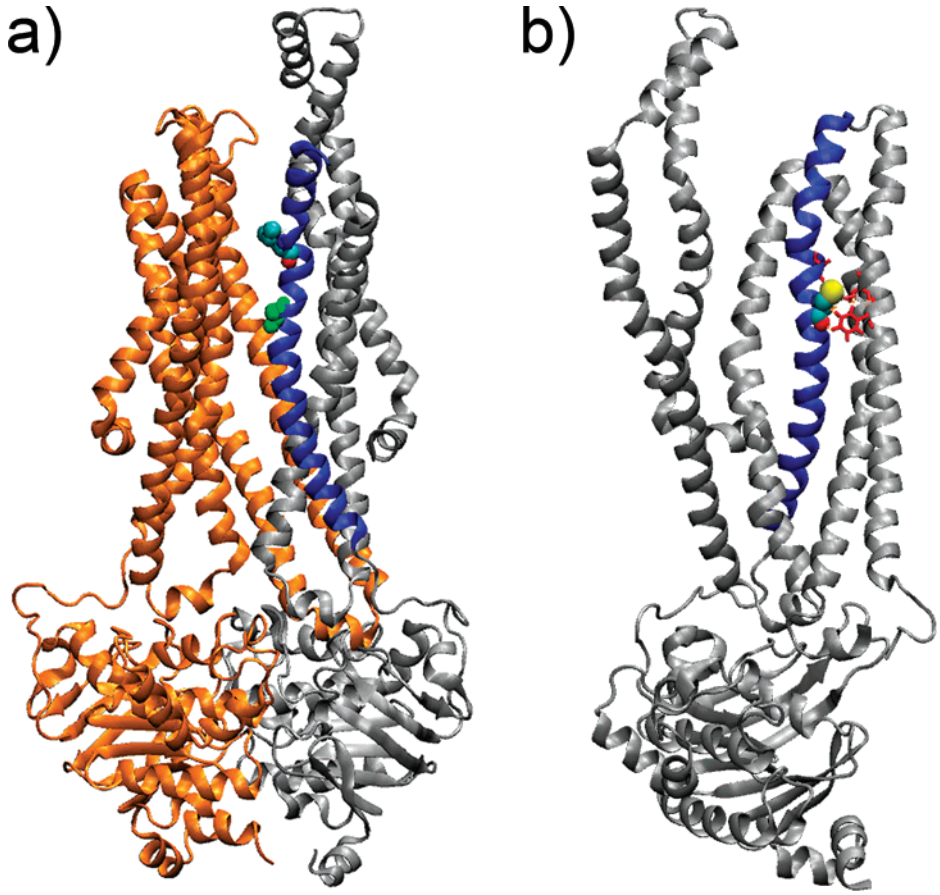


FIGURE 7: Homology model of TM6/P-gp. (a) Side view of the native P-gp homology model. TM4 and 5 have been removed for clarity. The N-terminal half is colored gray and the C-terminal half orange. TM6 (blue) contains a noticeable bend. The hydrogen-bonding pattern of TM6 is disrupted in the area surrounding the solvent-accessible L339 (CPK spacefill). G346 (green spacefill atoms) protrudes directly into a solvent-accessible cavity between TM5 and TM6. (b) Front view of the N-terminal half of the mutant P-gp model shows that the G346C side chain (CPK spacefill) is closely coordinated by one residue from TM6, A342 (red liquorice), and two residues from TM5, F303 (lower) and I306 (upper red liquorice). A342 and I306 sterically constrain G346C, while hydrogen bonds are formed between G346C and F303. Conformational stabilization due to this mutation is discussed in the text.

and I306 (TM5), as illustrated in Figure 7b. This increases the number of TM5−TM6 interfacial contacts (*44*, *45*), which might influence the movement of TM6.

## DISCUSSION

The cysteine-scanning mutagenesis investigations with TM6 clearly demonstrate that this helix plays an integral role in the translocation pathway of P-gp. TM6 may influence this pathway by contributing to the drug binding site or possibly through mediating the inter-domain communication with the NBDs. A previous study has demonstrated that the function of P-gp was unaffected by mutations of residues 331−343 to cysteine (*29*), although conjugation of residue 339C with coumarin-maleimide perturbed communication to the NBDs and impaired the rate of ATP hydrolysis in the presence of substrate. The present investigation focused on residues 344−360, which comprise the cytosolic half of TM6 and its extension linking to the N-terminal NBD. In our selection of residues for mutation, we wished to include residues at the intracellular end of TM6 as well as some residues in the cytosolic extension (which is also α-helical in conformation in Sav1866 (*33*)). Of the residues examined, only the mutation of G346 caused a significant reduction in the transport activity of P-gp due primarily to a reduction in the rate of ATP hydrolysis. The reduction of ATPase activity by the mutation of residue 346 to cysteine has been previously observed, although the underlying mechanism was not explored (*25*).

Contrary to expectations, the reduced ATPase activity was caused by reduction in the basal activity *per se*. There were also effects on the stimulation of ATP hydrolysis, but these were drug-dependent. For example, the modulator nicardipine stimulated hydrolysis to an identical extent and at a similar potency in the G346C isoform compared that in the cysteine-less isoform. In contrast, the substrate vinblastine did not produce any stimulation following the mutation. This data could suggest that the residue G346 contributes to the vinblastine and not to the nicardipine binding site. Interestingly, the two compounds have been shown to interact at pharmacologically distinct sites on the protein (*7*, *46*). However, both compounds displayed unaltered binding to the protein, indicating that the mutation was not within the nicardipine or vinblastine binding sites. This therefore suggests that the two binding sites communicate to the NBDs via distinct pathways, rather than through a common route. This accounts for the unaffected nicardipine stimulation, reduced vinblastine stimulation, and yet unaffected vinblastine binding to G346C mutant. A similar conclusion was demonstrated for the Q347C and S349C isoforms (Tables 3 and 4) and was also shown for the L339C isoform (*29*).

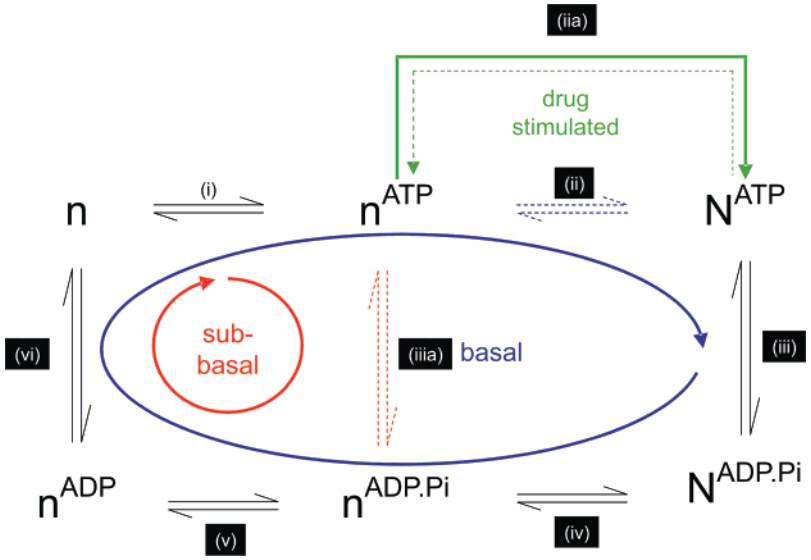


FIGURE 8: Catalytic cycle for P-gp, the influence of the G346C mutation. The possible routes comprising the ATP hydrolytic pathway of P-gp are depicted in the schematic. NBDs that are associated into a sandwich dimer (such that their signature motifs are coordinated for ATP binding) are shown as N, while n refers to NBD(s) that are not associated in this manner. Routes A (red) and B (blue) are the pathways for sub-basal and basal ATP hydrolysis by the protein (discussed in the text), while route C (green) indicates the acceleration of NBD sandwich dimerization that is promoted by the drug substrate.

The spatial proximity and respective localization of the drug binding sites on P-gp have not yet been resolved, although a range of distinct biochemical and pharmacological approaches have demonstrated that multiple interaction sites exist (*7*, *10*, *11*, *13*). Similarly, the amino acids involved in mediating communication to the NBDs remain unresolved, although structural information from Sav1866 (*33*) and BtuCD (*47*) transporters suggest that segments linking transmembrane helices or segments between TM6 and NBD1 and/ or TM12 and NBD2 are responsible. Medium resolution structural information of P-gp confirms that the TM helices extend beyond the regions encompassed by the membrane bilayers (*30*), supporting direct communication between TM segments and the NBDs.

The fact that the primary effect of the G346C mutation is a reduction in basal ATP hydrolysis appears counter-intuitive since the mutated residue lies within the TMD, while ATP hydrolysis occurs at the NBDs. The reduction in basal activity suggests that TM6 can dictate or influence events in the NBDs even in the absence of any drug substrate. This is not without precedent since TMDs have been shown to greatly influence the activity of NBDs; for example, the rates of ATP hydrolysis by isolated NBDs are dramatically reduced (by as much as 10-fold) compared to those observed when associated with TMDs for a number of ABC transporters (*48*−*53*). As shown in Figure 8, ATP hydrolysis comprises multiple discrete steps and one, or more, will be affected by the G346C mutation. Our data demonstrates that ATP binding (i.e., step (i)) is unaffected by mutation, and similarly, the release of ADP (step (vi)) is likely to remain intact since the affinity for the dinucleotide to bind was also unaltered. Phosphate release (step (v)) and the hydrolytic reaction (step (iii)) are unlikely to represent the rate-limiting step based on thermodynamic considerations (i.e., both are exergonic reactions). The most likely candidate is the so-called sandwich dimerization of NBDs (step (ii), hereafter referred to as signature motif coordination), a step which is thought to be essential for ATP hydrolysis by all ABC transporters. Dimerization of the NBDs encloses ATP such that it is coordinated between the P-loop of one monomer and the signature sequence of the opposing partner. Drug binding is believed to accelerate the rate of ATP hydrolysis by facilitating this event (*54*); in other words, it increases the rate of step (ii), shown as step (iia) in Figure 8.

The signature motif coordination of NBDs may be the rate-limiting step of the catalytic cycle, but how does the G346C mutation affect it, and is it required for basal ATP hydrolysis? On the basis of the nucleotide sandwich model for ATP hydrolysis (*55*), basal ATPase activity is likely to precede the signature motif coordination of NBDs. As mentioned above, the lower rate of hydrolysis under drug-free (basal) conditions is due to the slow rate of step (ii) and occurs via route B (Figure 8). An alternative sequence of events may follow the path (i) → (iiia) → (v) → (vi), dubbed sub-basal route A in Figure 8, in which NBDs may still be dimerized but whose signature motifs are not coordinated for ATP hydrolysis, or a mixture of the two pathways. The influence of the TMD may therefore be to limit progression through step (ii). This may be the nature of coupling between the two domains. The G346C mutation prevents conformational changes within the TMD such that basal route B occurs at a slower rate or alternatively, prevents step (ii) from occurring, and the protein proceeds via sub-basal route A. In addition, the G346C mutation prevents step (iia) (drug-stimulated ATP hydrolysis) from occurring for vinblastine but not nicardipine. This suggests that vinblastine communicates to the NBD(s) via an alternative pathway mediated via residue G346. In order to provide a theoretical visualization (as opposed to a structure-based interpretation, which remains impossible) of the G346C mutation, we have constructed a P-gp homology model based upon the structure of Sav1866. The structure-based comparison of the X-ray crystallographic data for Sav1866 (*33*) with the 8 Å electron microscopy data for P-gp (*30*) demonstrates that several of the long α-helices in Sav1866 can be superimposed onto long rod-shaped EM densities observed by electron microscopy of 2D P-gp

crystals (Ford, R., personal communication). This, together with the ease of alignment of P-gp with Sav1866 (i.e., the length and separation of the TM α-helices are highly similar), supports the use of Sav1866 as a template structure for a P-gp homology model. Our model indicates that the presence of a cysteine at residue 346 gives rise to a steric interaction between TM5 and TM6, sandwiching 346C between A342, F303, and I306 and increasing the number of inter-helix contacts between TM5 and TM6. We propose that this interaction between TM5 and TM6 impedes motion in the cytosolic half of TM6, hindering the TMD/NBD communication, NBD signature motif coordination, and ATP hydrolysis through the basal route B. Further *in silico* mutations of G346 indicate that helix interactions between G346 and TM5 are both charge and volume-dependent, although more computational and experimental analysis would be required to fully delineate this.

In the present article, we demonstrate that the TMDs of P-gp play a major role in regulating the rate of ATP hydrolysis in the NBDs, which is consistent with a previous model for ABC transporters (*55*). Moreover, the regulation may be perturbed by the G346C mutation in TM6, suggesting a key role for this region of the protein for both the basal- and drug-stimulated activity. The rate-limiting step in ATP hydrolysis by P-gp (and other ABC transporters) is assumed to be the signature motif coordination of NBDs, and the G346C mutation in TM6 may retard the rate of this step.

## ACKNOWLEDGMENT

We thank Dr. Tony George for the critical reading of the manuscript and Dr. Kenneth Linton for assistance with the production of recombinant baculovirus.

## REFERENCES

1. Chan, H. S., Haddad, G., Thorner, P. S., DeBoer, G., Lin, Y. P., Ondrusek, N., Yeger, H., and Ling, V. (1991) P-glycoprotein expression as a predictor of the outcome of therapy for neuroblastoma, *N. Engl. J. Med. 325*, 1608−1614.
2. van den Heuvel-Eibrink, M. M., Sonneveld, P., and Pieters, R. (2000) The prognostic significance of membrane transport-associated multidrug resistance (MDR) proteins in leukemia, *Int. J. Clin. Pharmacol. Ther. 38*, 94−110.
3. Cordon-Cardo, C., O'Brien, J. P., Casals, D., Rittman-Grauer, L., Biedler, J. L., Melamed, M. R., and Bertino, J. R. (1989) Multidrug-resistance gene (P-glycoprotein) is expressed by endothelial cells at blood-brain barrier sites, *Proc. Natl. Acad. Sci. U.S.A. 86*, 695−698.
4. van der Valk, P., van Kalken, C. K., Ketelaars, H., Broxterman, H. J., Scheffer, G., Kuiper, C. M., Tsuruo, T., Lankelma, J., Meijer, C. J., Pinedo, H. M., et al. (1990) Distribution of multi-drug resistance-associated P-glycoprotein in normal and neoplastic human tissues. Analysis with 3 monoclonal antibodies recognizing different epitopes of the P-glycoprotein molecule, *Ann. Oncol. 1*, 56−64.
5. Cascorbi, I. (2006) Role of pharmacogenetics of ATP-binding cassette transporters in the pharmacokinetics of drugs, *Pharmacol. Ther. 112*, 457−473.
6. Dey, S., Ramachandra, M., Pastan, I., Gottesman, M. M., and Ambudkar, S. V. (1997) Evidence for two nonidentical drug-interaction sites in the human P- glycoprotein, *Proc. Natl. Acad. Sci. U.S.A. 94*, 10594−10599.
7. Martin, C., Berridge, G., Higgins, C. F., Mistry, P., Charlton, P., and Callaghan, R. (2000) Communication between multiple drug binding sites on P-glycoprotein, *Mol. Pharmacol. 58*, 624−632.
8. Pascaud, C., Garrigos, M., and Orlowski, S. (1998) Multidrug resistance transporter P-glycoprotein has distinct but interacting binding sites for cytotoxic drugs and reversing agents, *Biochem. J. 333*, 351−358.
9. Shapiro, A. B., and Ling, V. (1997) Positively cooperative sites for drug transport by P-glycoprotein with distinct drug specificities, *Eur. J. Biochem. 250*, 130−137.
10. Bruggeman, E. P., Germann, U. A., Gottesman, M. M., and Pastan, I. (1989) Two different regions of phosphoglycoprotein are photoaffinity labeled by azidopine, *J. Biol. Chem. 264*, 15483−15488.
11. Ecker, G. F., Csaszar, E., Kopp, S., Plagens, B., Holzer, W., Ernst, W., and Chiba, P. (2002) Identification of ligand-binding regions of P-glycoprotein by activated-pharmacophore photoaffinity labeling and matrix-assisted laser desorption/ionization-time-of-flight mass spectrometry, *Mol. Pharmacol. 61*, 637−648.
12. Greenberger, L. M. (1993) Major photoaffinity drug labeling sites for iodoaryl azidoprazosin in P-glycoprotein are within, or immediately C-terminal to, transmembrane domains 6 and 12, *J. Biol. Chem. 268*, 11417−11425.
13. Pleban, K., Kopp, S., Csaszar, E., Peer, M., Hrebicek, T., Rizzi, A., Ecker, G. F., and Chiba, P. (2005) P-glycoprotein substrate binding domains are located at the transmembrane domain/transmembrane domain interfaces: a combined photoaffinity labeling-protein homology modeling approach, *Mol. Pharmacol. 67*, 365−374.
14. Taylor, A. M., Storm, J., Soceneantu, L., Linton, K. J., Gabriel, M., Martin, C., Woodhouse, J., Blott, E., Higgins, C. F., and Callaghan, R. (2001) Detailed characterization of cysteine-less P-glycoprotein reveals subtle pharmacological differences in function from wild-type protein, *Br. J. Pharmacol. 134*, 1609−1618.
15. al-Shawi, M. K., Urbatsch, I. L., and Senior, A. E. (1994) Covalent inhibitors of P-glycoprotein ATPase activity, *J. Biol. Chem. 269*, 8986−8992.
16. Hrycyna, C. A., Ramachandra, M., Germann, U. A., Cheng, P. W., Pastan, I., and Gottesman, M. M. (1999) Both ATP sites of human P-glycoprotein are essential but not symmetric, *Biochem. 38*, 13887−13899.
17. Loo, T. W., and Clarke, D. M. (1995) Covalent modification of human P-glycoprotein mutants containing a single cysteine in either nucleotide-binding fold abolishes drug- stimulated ATPase activity, *J. Biol. Chem. 270*, 22957−22961.
18. Callaghan, R., Ford, R. C., and Kerr, I. D. (2006) The translocation mechanism of P-glycoprotein, *FEBS Lett. 580*, 1056−1063.
19. Devine, S. E., Ling, V., and Melera, P. W. (1992) Amino acid substitutions in the sixth transmembrane domain of P- glycoprotein alter multidrug resistance, *Proc. Natl. Acad. Sci. U.S.A. 89*, 4564−4568.
20. Loo, T. W., and Clarke, D. M. (1994) Mutations to amino acids located in predicted transmembrane segment 6 (TM6) modulate the activity and substrate specificity of human P- glycoprotein, *Biochemistry 33*, 14049−14057.
21. Loo, T. W., and Clarke, D. M. (1996) Inhibition of oxidative cross-linking between engineered cysteine residues at positions 332 in predicted transmembrane segments (TM) 6 and 975 in predicted TM12 of human P-glycoprotein by drug substrates, *J. Biol. Chem. 271*, 27482−27487.
22. Ma, J. F., Grant, G., and Melera, P. W. (1997) Mutations in the sixth transmembrane domain of P-glycoprotein that alter the pattern of cross-resistance also alter sensitivity to cyclosporin A reversal, *Mol. Pharmacol. 51*, 922−930.
23. Song, J., and Melera, P. W. (2001) Further characterization of the sixth transmembrane domain of Pgp1 by site-directed mutagenesis, *Cancer Chemother. Pharmacol. 48*, 339−46.
24. Loo, T. W., Bartlett, M. C., and Clarke, D. M. (2003) Substrate-induced conformational changes in the transmembrane segments of human P-glycoprotein. Direct evidence for the substrate-induced fit mechanism for drug binding, *J. Biol. Chem. 278*, 13603−13606.
25. Loo, T. W., and Clarke, D. M. (1997) Identification of residues in the drug-binding site of human P- glycoprotein using a thiol-reactive substrate, *J. Biol. Chem. 272*, 31945−31948.
26. Loo, T. W., and Clarke, D. M. (1999) Identification of residues in the drug-binding domain of human P-glycoprotein. Analysis of transmembrane segment 11 by cysteine-scanning mutagenesis and inhibition by dibromobimane, *J. Biol. Chem. 274*, 35388−35392.
27. Rothnie, A., Storm, J., Campbell, J., Linton, K. J., Kerr, I. D., and Callaghan, R. (2004) The topography of transmembrane segment six is altered during the catalytic cycle of P-glycoprotein, *J. Biol. Chem. 279*, 34913−34921.
28. Loo, T. W., and Clarke, D. M. (2001) Defining the drug-binding site in the human multidrug resistance P-glycoprotein using a

methanethiosulfonate analog of verapamil, MTS-verapamil, *J. Biol. Chem. 276*, 14972−14979.
29. Rothnie, A., Storm, J., McMahon, R., Taylor, A., Kerr, I. D., and Callaghan, R. (2005) The coupling mechanism of P-glycoprotein involves residue L339 in the sixth membrane spanning segment, *FEBS Lett. 579*, 3984−3990.
30. Rosenberg, M. F., Callaghan, R., Modok, S., Higgins, C. F., and Ford, R. C. (2005) Three-dimensional Structure of P-glycoprotein: the transmembrane regions adopt an asymmetric configuration in the nucleotide-bound state, *J. Biol. Chem. 280*, 2857−2862.
31. Rosenberg, M. F., Kamis, A. B., Callaghan, R., Higgins, C. F., and Ford, R. C. (2003) Three-dimensional structures of the mammalian multidrug resistance P-glycoprotein demonstrate major conformational changes in the transmembrane domains upon nucleotide binding, *J. Biol. Chem. 278*, 8294−8299.
32. Rosenberg, M. F., Velarde, G., Ford, R. C., Martin, C., Berridge, G., Kerr, I. D., Callaghan, R., Schmidlin, A., Wooding, C., Linton, K. J., and Higgins, C. F. (2001) Repacking of the transmembrane domains of P-glycoprotein during the transport ATPase cycle, *EMBO J. 20*, 5615−5625.
33. Dawson, R. J., and Locher, K. P. (2006) Structure of a bacterial multidrug ABC transporter, *Nature 443*, 180−185.
34. Stenham, D. R., Campbell, J. D., Sansom, M. S., Higgins, C. F., Kerr, I. D., and Linton, K. J. (2003) An atomic detail model for the human ATP binding cassette transporter P-glycoprotein derived from disulfide cross-linking and homology modeling, *FASEB J. 17*, 2287−2289.
35. Chifflet, S., Chiesa, U. T. R., and Tolosa, S. (1988) A method for the determination of inorganic phosphate in the presence of labile organic phosphate and high concentrations of protein: application to lens ATPases, *Anal. Biochem. 168*, 1−4.
36. Gabriel, M. P., Storm, J., Rothnie, A., Taylor, A. M., Linton, K. J., Kerr, I. D., and Callaghan, R. (2003) Communication between the nucleotide binding domains of P-glycoprotein occurs via conformational changes that involve residue 508, *Biochemistry 42*, 7780−7789.
37. Notredame, C., Higgins, D. G., and Heringa, J. (2000) T-Coffee: a novel method for fast and accurate multiple sequence alignment, *J. Mol. Biol. 302*, 205−217.
38. Thompson, J. D., Higgins, D. G., and Gibson, T. J. (1994) CLUSTAL W: improving the sensitivity of progressive multiple sequence alignment through sequence weighting, position-specific gap penalties and weight matrix choice, *Nucleic Acids Res. 22*, 4673−4680.
39. Rost, B., Liu, J., Nair, R., Wrzeszczynski, K. O., and Ofran, Y. (2003) Automatic prediction of protein function, *Cell. Mol. Life Sci. 60*, 2637−2650.
40. Sali, A., Potterton, L., Yuan, F., van Vlijmen, H., and Karplus, M. (1995) Evaluation of comparative protein modeling by MODELLER, *Proteins 23*, 318−326.
41. Laskowski, R. A., Moss, D. S., and Thornton, J. M. (1993) Main-chain bond lengths and bond angles in protein structures, *J. Mol. Biol. 231*, 1049−1067.
42. Vriend, G. (1990) WHAT IF: a molecular modeling and drug design program, *J. Mol. Graphics 8*(1): 52−56, 29.
43. Rothnie, A., Theron, D., Soceneantu, L., Martin, C., Traikia, M., Berridge, G., Higgins, C. F., Devaux, P. F., and Callaghan, R. (2001) The importance of cholesterol in maintenance of P-glycoprotein activity and its membrane perturbing influence, *Eur. Biophys. J. 30*, 430−442.
44. Senes, A., Gerstein, M., and Engelman, D. M. (2000) Statistical analysis of amino acid patterns in transmembrane helices: the GxxxG motif occurs frequently and in association with beta-branched residues at neighboring positions, *J. Mol. Biol. 296*, 921−936.
45. Russ, W. P., and Engelman, D. M. (2000) The GxxxG motif: a framework for transmembrane helix-helix association, *J. Mol. Biol. 296*, 911−919.
46. Ferry, D. R., Russell, M. A., and Cullen, M. H. (1992) P-glycoprotein possesses a 1,4-dihydropyridine selective drug acceptor site which is allosterically coupled to a vinca alkaloid selective binding site, *Biochem. Biophys. Res. Commun. 188*, 440−445.
47. Locher, K. P., Lee, A. T., and Rees, D. C. (2002) The E. coli BtuCD structure: a framework for ABC transporter architecture and mechanism, *Science 296*, 1091−1098.
48. Berridge, G., Walker, J. A., Callaghan, R., and Kerr, I. D. (2003) The nucleotide-binding domains of P-glycoprotein. Functional symmetry in the isolated domain demonstrated by N-ethylmaleimide labeling, *Eur. J. Biochem. 270*, 1483−1492.
49. Davidson, A. L., and Nikaido, H. (1991) Purification and characterization of the membrane-associated components of the maltose transport system from *Escherichia coli*, *J. Biol. Chem. 266*, 8946−8951.
50. Ko, Y. H., and Pedersen, P. L. (1995) The first nucleotide binding fold of the cystic fibrosis transmembrane conductance regulator can function as an active ATPase, *J. Biol. Chem. 270*, 22093−22096.
51. Liu, P.-Q., and Ames, G. F.-L. (1998) *In vitro* disassembly and reassembly of an ABC transporter, the histidine permease, *Proc. Natl. Acad. Sci. U.S.A. 95*, 3495−3500.
52. Morbach, S., Tebbe, S., and Schneider, E. (1993) The ATP-binding cassette (ABC) transporter for maltose/maltodextrins of *Salmonella typhimurium*, *J. Biol. Chem. 268*, 18617−18621.
53. Nikaido, K., Liu, P.-Q., and Ames, G. F.-L. (1997) Purification and characterization of HisP, the ATP-binding subunit of a traffic ATPase (ABC transporter), the histidine permease of *Salmonella typhimurium*, *J. Biol. Chem. 272*, 27745−27752.
54. Tombline, G., Muharemagic, A., White, L. B., and Senior, A. E. (2005) Involvement of the "occluded nucleotide conformation" of p-glycoprotein in the catalytic pathway, *Biochemistry 44*, 12879−12886.
55. Jones, P. M., and George, A. M. (2002) Mechanism of ABC transporters: a molecular dynamics simulation of a well characterized nucleotide-binding subunit, *Proc. Natl. Acad. Sci. U.S.A. 99*, 12639−12644.

BI700447P